Express Polymer Letters Vol.17, No.8 (2023) 789–805
Available online at www.expresspolymlett.com
https://doi.org/10.3144/expresspolymlett.2023.59

Research article

Development of biodegradable PLA composites and tangerine peel flour with improved toughness containing a natural-based terpenoid

Jaume Gomez-Caturla[1*], *Nestor Montanes*[1], *Luis Quiles-Carrillo*[1], *Rafael Balart*[1], *Daniel Garcia-Garcia*[1], *Franco Dominici*[2], *Debora Puglia*[2], *Luigi Torre*[2]

[1]Technological Institute of Materials (ITM), Universitat Politècnica de València (UPV), Plaza Ferrándiz y Carbonell 1, 03801 Alcoy, Spain
[2]Dipartimento di Ingegneria Civile ed Ambientale, University of Perugia, UdR INSTM, Strada di Pentima, 4-05100 Terni (TR) Italy

Received 11 February 2023; accepted in revised form 20 April 2023

Abstract. The present work reports on the development of environmentally friendly, completely biodegradable wood plastic composites based on polylactide (PLA) and tangerine peel flour (TPF), plasticized by α-terpinyl acetate (TA). The TPF varied in the 10–30 wt% while the PLA to TA (wt%/wt%) was set to 4 (*i.e.*, 25 wt% TA plasticizer was added with regard to the PLA wt%). The developed composites were processed by extrusion and injection molding. The composites presented excellent elongation at break, achieving values of 300% for the PLA+TA sample. Elongation at break values of 200% for the PLA composite with 10 wt% TPF and plasticized with TA were obtained. Those results were confirmed by the appearance of filament-like structures observed in field emission scanning electron microscopy images. Differential scanning calorimetry and dynamic mechanical thermal analysis revealed a remarkable decrease in the glass transition temperature of PLA as a result of the plasticizing effect of TA. Glass transition was reduced from 63 °C down to 41 °C approximately. This implied an increase in the ductility of the material. The samples with TPF exhibited a dark brown color, making them perfect for wood plastic composite applications. Water contact angle results show that TA and TPF change the wetting properties of the obtained composites. A general decrease in the water contact angle was observed with the addition of TPF and TA. Finally, disintegration tests proved that the developed composites are fully biodegradable. All the samples except for neat PLA achieved 100% disintegration in controlled compost soil conditions after 5 weeks, while neat PLA reached complete disintegration in 6 weeks.

Keywords: *polylactide, tangerine peel flour, α-terpinyl acetate, plasticization, wood plastic composites, biodegradable*

---

1. Introduction

In the last decades, the environmental issues provoked by the extended use of petrochemical polymers, such as an increase in the carbon footprint and a great amount of generated waste, have risen social and scientific awareness related to the use of these polymers. Therefore, more environmentally friendly polymers and materials have attracted great attention in this field. One of the most popular examples is the development of wood plastic composites (WPC), which arise as an alternative to wood-based products [1]. These kinds of materials are based on a thermoplastic polymer matrix, such as polypropylene (PP), polylactide (PLA), or polyethylene (PE), among others, and fillers obtained from the food and agroforestry industry. At first, the most popular fillers were sawdust and wood fibers [2]. However, other alternative fillers have been proposed in the last years, such as lignocellulosic fillers from the food industry, including fruit peels, seeds, and other wastes

---

[*] Corresponding author, e-mail: jaugoca@epsa.upv.es

[3, 4]. These fillers allow reducing the cost of the material, as they are obtained from wastes and are far cheaper than the neat polymer itself. Depending on the fruit, the amount of by-products ranges from 10 to 60 wt%, so using those by-products as fillers in polymer technology helps to upgrade them and even provide polymers with additional properties, such as enhanced mechanical resistance, biodegradability, antioxidant activity, antimicrobial properties, or even different colors [5, 6].

Polylactide is a biobased biodegradable linear aliphatic polyester. Lactic acid is its main monomer, which is obtained from the fermentation of starch-rich sources (rice, sugarcane, potato, corn, and so on) [7]. This thermoplastic polymer is considered one of the most promising materials in the bioplastics market, with an annual production of 140 000 tons [8]. Its most attractive properties are its biodegradability and its renewable origin. However, composites based on this polymer matrix present some limitations in terms of ductility, as PLA itself is a brittle polymer, and this brittleness is more pronounced in PLA-lignocellulosic fillers, characterized by a low impact strength and toughness [9]. Despite there are several technical solutions to this drawback, a widely and cost-effective technical solution is the use of plasticizers that increase its ductility. Another methodology is blending PLA with other flexible polymers [10, 11]. The use of biobased plasticizers is becoming especially important and interesting these days, as they are very cost effective and efficient and help to preserve the environmentally friendly nature of PLA. These plasticizers mainly help to increase the chain mobility of the polymer matrix by increasing the free volume in PLA. Low molecular weight natural plasticizers such as cardanol are preferred due to their high plasticizing effectiveness [12, 13]. Plasticizers are preferred instead of copolymer synthesis due to their ability to reduce the glass transition temperature of PLA, increasing its toughness and overall ductile properties [14, 15].

Tangerine (*Citrus reticulata*) is one of the most by-product-generating crops, being its peel the main waste produced in the tangerine industry. This waste possesses great amounts of cellulose, lignin, and hemicellulose, which are essential components for defining a lignocellulosic filler, similar to wood flour fillers [16, 17]. Tangerine peel has a composition of around 4 wt% essential oils [18, 19], which possess several interesting chemical compounds. These compounds include terpenes and terpenoids, such as D-limonene, β-myrcene, α-pinene, γ-terpinene, and linalool [20]. These compounds generally present great antioxidant, antimicrobial and antifungal activities, and have proved to provide some plasticization to PLA.

Some research works have studied the possibility of combining citric waste fillers, such as orange peel flour, into thermoplastic polymers, such as poly(vinyl alcohol) (PVA) [21] or low-density polyethylene (LDPE) [22]. Nonetheless, hardly any study has been carried out related to the use of tangerine peel flour as a filler for thermoplastic composites, especially polylactide. Hejna *et al.* [20] developed wood plastic composites based on high-density polyethylene (HDPE) with tangerine peel flour, which gave the polymer enhanced thermal stability, mechanical strength, and flowability.

In this study, tangerine peel flour (TPF) is used as a lignocellulosic filler for developing environmentally friendly wood plastic composites based on polylactide. Considering that tangerine peel has not been extendedly studied in the field of composites, several amounts of tangerine peel flour, ranging from 10 to 30 wt% (with regard to PLA) have been used in the study. Additionally, α-terpinyl acetate (TA), which is a natural plasticizer originating from citric acid, is utilized in order to reduce the brittleness of PLA and its composites with TPF. TA and tangerine peel are expected to have a certain synergy, as TA is derived from citric fruits and is a monoterpenoid [23]. This fact makes TA possess a great affinity for TPF, as it has terpenes and terpenoids in its composition, as stated before. Therefore, plasticized and unplasticized wood plastic composites have been produced, and their properties have been evaluated according to theoretical solubility parameters, tensile tests, and fracture surface morphology observation by field emission scanning electron microscopy (FESEM). The main thermal properties of the developed PLA composites were obtained by differential scanning calorimetry (DSC), thermogravimetric analysis (TGA), and dynamic-mechanic-thermal analysis (DMTA). Moreover, the surface appearance and wettability were measured by colorimetry and water drop goniometry.

2. Materials and methods

2.1. Materials

Bio-based PLA Purapol L130 grade was supplied by Corbion Purac (The Netherlands, Amsterdam), with a density of 1.24 g/cm^3, a melt flow index of 16 g/10 min (at 210 °C/2.16 kg), and a melting temperature of 175 °C.

Tangerines from the Clemenvilla variety were purchased from the local market in Alcoy, Spain. α-terpinyl acetate (TA) (Product Code: 1003313906) was supplied by Sigma Aldrich. Tangerines were peeled, and the peels were first dried at 45 °C for 48 h in a dehumidifying stove (MCP Vacuum Casting System, Lubeck, Germany) to remove residual moisture. Then, the peels were milled in a ZM 200 centrifugal mill from Retsch (Düsseldorf, Germany) at a speed of 8000 rpm and finally sieved with a 300 µm mesh filter. Thus, tangerine peel flour was obtained (TPF). Figure 1 illustrates the field emission scanning electron microscopy (FESEM) image of TPF, as well as the distribution of the particle size. The average diameter of the particles was 25 µm, approximately, as obtained from FESEM study.

2.2. Processing of PLA/TPF composites

PLA and TPF were initially dried at 40 °C for 48 h in a dehumidifying dryer MDEO to remove any residual moisture prior to processing. Thereafter, the corresponding proportions of each component, including the α-terpinyl acetate plasticizer, were mixed and homogenized. Table 1 shows the composition of each developed formulation, the plasticizer content was kept constant with regard to PLA wt%. In particular, the wt% PLA to wt% plasticizer ratio was 4 for all compositions (*i.e.* 25 wt% plasticizer was added with regard to the wt% PLA). The formulations were compounded by an extrusion process in a twin-screw extruder from Construcciones Mecánicas Dupra, S.L. (Alicante, Spain). This extruder has a 25 mm diameter with a length-to-diameter ratio (*L*/*D*) of 24. The extrusion process was carried out at a rate of 22 rpm, with a temperature profile from the hopper to the die of 170–175–180–185 °C. The compounded materials were pelletized using an air-knife unit. In all cases, residence time was approximately 1 min.

Table 1. Compositions of the developed formulations of PLA/TPF with TA plasticizer.

Code	PLA [wt%]	TPF [wt%]	TA [phr]
PLA	100	0	0
PLA+10TPF	90	10	0
PLA+10TPF+22.5TA	90	10	22.5
PLA+20TPF+20TA	80	20	20
PLA+30TPF+17.5TA	70	30	17.5
PLA+20TA	80	0	20*

*This composition means 20 wt% instead of 20 phr.

Pellets were shaped into standard samples using a Meteor 270/75 injection molding machine from Mateu & Solé (Barcelona, Spain). The temperature profile in the injection molding unit was 175 °C (hopper), 180, 185, and 190 °C (injection nozzle). This injection unit was operated with a clamping force of 75 tons. Other processing parameters, such as the filling and cooling times were set to 1 and 10 s, respectively. Standard samples for mechanical and thermal characterization with an average thickness of 4 mm were obtained.

2.3. Characterization of PLA/TPF composites

2.3.1. Theoretical analysis of the PLA/plasticizer interaction

In the process of plasticization, the solubility of the selected plasticizer in the chosen polymer plays a very important role. In this work, the group-contribution method developed by van Krevelen and Hoftyzer was

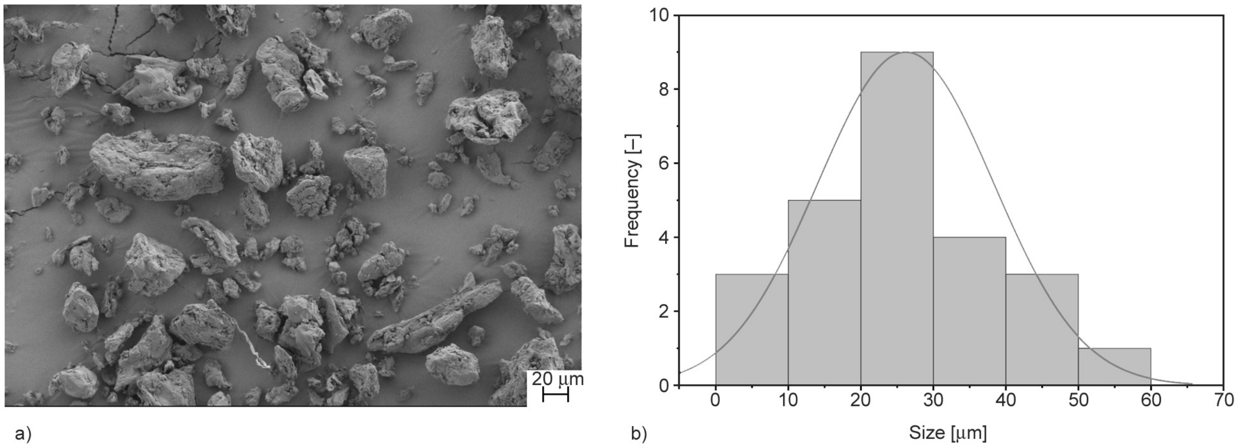

Figure 1. Tangerine peel flour morphology (TPF) a) FESEM image at 250× magnification of TPF, b) histogram of the particle size of TPF.

used to calculate the solubility parameter (δ). Its main contributions were also calculated, which are related to the dispersion forces (δ_d), polar forces (δ_p), and hydrogen bonding (δ_h) (see Equation (1)):

$$\delta = \delta_d^2 + \delta_p^2 + \delta_h^2 \tag{1}$$

As proposed by van Krevelen and Hoftyzer, the three solubility components can be estimated from group contributions as indicated by Equations (2) to (4):

$$\delta_d = \frac{\sum F_{di}}{V} \tag{2}$$

$$\delta_p = \frac{\sqrt{\sum F_{pi}^2}}{V} \tag{3}$$

$$\delta_h = \sqrt{\frac{\sum E_{hi}}{V}} \tag{4}$$

The F-method, based on the molar attraction constants, is quite accurate for predicting the dispersive and polar contributions (δ_d, and δ_p, respectively) as indicated in Equations (2) and (3), respectively. However, the F-method cannot be applied to the hydrogen bonding component (δ_h). Hansen concluded that the hydrogen bonding energy (E_{hi}) per structural group could be considered almost constant. Considering the structure and the group contribution proposed by van Krevelen and Hoftyzer [24], the solubility components are gathered in Table 2. Additionally, Table 2 includes the R_a parameter, which is indicative of the distance existing between the solubility coordinates of the plasticizer in relation to neat PLA. R_a has been calculated according to Equation (5), where the constant 4 in the first term was obtained from plots of experimental data to define spherical solubility regions rather than spheroidal regions. If R_a (the distance) equals zero, it means that both plasticizer and polymer are thermodynamically similar, which leads to great affinity and good solubility. As expected, the greater the distance, the lower the solubility. When a certain distance threshold is surpassed, the solubility becomes negligible. This distance is related to the polymer radius (or sphere radius), R_0, which defines a spherical solubility region of a polymer. The center of the sphere is defined by the three solubility parameters δ_d, δ_p, and δ_h:

$$R_a = \sqrt{4\left(\delta_{d_{plast}} - \delta_{d_{PLA}}\right)^2 + \left(\delta_{p_{plast}} - \delta_{p_{PLA}}\right)^2 + \left(\delta_{h_{plast}} - \delta_{h_{PLA}}\right)^2} \tag{5}$$

Table 2. Theoretical approach for the solubility of polylactide (PLA) formulations with α-terpinyl acetate.

Material	**δ_d [MPa$^{1/2}$]**	**δ_p [MPa$^{1/2}$]**	**δ_h [MPa$^{1/2}$]**	**δ [MPa$^{1/2}$]**	**R_a [MPa$^{1/2}$]**	***RED***
PLA	15.33	8.44	10.98	20.66	–	
α-terpinyl acetate (TA)	15.34	2.38	5.83	16.58	6.57	0.61

The relative energy difference (*RED*) is also calculated, and it is defined as the relation between R_a and the solubility sphere radius of neat PLA, R_0, which is 10.7 MPa$^{1/2}$ (Equation (6)) [25]. The closer the *RED* value is to zero, the better the miscibility between PLA and the chosen plasticizer. When the *RED* parameter is close to 1, it means the plasticizer and the polymer are at the threshold of good affinity, whereas *RED* values greater than 1 indicate a poor affinity between them. Brüster *et al.* [26] reported *RED* values of 0.93 and 0.99 for limonene and myrcene in PLA-plasticized formulations. Despite the *RED* values being close to 1, they observed that limonene, with a lower *RED* value, gave PLA more efficient plasticization than myrcene, which RED value was very close to the solubility borderline:

$$RED = \frac{R_a}{R_0} \tag{6}$$

As it is denoted by the values in Table 2, α-terpinyl acetate possesses a great affinity for PLA, as its *RED* value is far below 1, thus proving their potential miscibility. This theoretical result will be verified by the results obtained in the experimental section.

2.3.2. Mechanical characterization

The tensile properties of the PLA/TPF composites were evaluated using a universal testing machine ELIB 50 from S.A.E. Ibertest (Madrid, Spain). The test was conducted following the instructions of ISO 527-1:2012. A 5 kN load cell was used while the cross-head speed was set to 5 mm/min. Tensile test specimens of dimensions 150×10×4 mm. The Shore D hardness was measured in a 676-D durometer from J. Bot Instruments (Barcelona, Spain) on 80×10×4 mm rectangular samples according to ISO 868:2003. The impact strength was studied on 80×10×4 mm rectangular samples in a Charpy pendulum (1-J) from Metrotec S.A. (San Sebastián, Spain) on notched samples (V-notch type with a radius of 0.25 mm), following ISO 179-1:2010. A minimum of 5 samples were tested for each material.

2.3.3. Field emission scanning electron microscopy (FESEM)

The surface morphology of the cross-section of fractured impact test samples was evaluated by field emission scanning electron microscopy (FESEM) using a ZEISS ULTRA 55 microscope from Oxford Instruments (Abingdon, United Kingdom). The samples were sputtered with a gold-palladium alloy in an EMITECH sputter coating SC7620 model from Quorum Technologies, Ltd. (East Sussex, UK). The microscope was operated with an acceleration voltage of 1.5 kV.

2.3.4. Thermal characterization

The main thermal properties of the PLA/TPF composites were obtained by means of differential scanning calorimetry (DSC) in a DSC 821 from Mettler-Toledo Inc. (Schwerzenbach, Switzerland). Samples weighed about 5–8 mg, and they were placed in 40 µl aluminum crucibles. Three thermal steps were applied to the samples: first, a heating cycle from 30 to 200 °C, then a cooling cycle down to 0 °C, and, finally, a second heating stage from 0 up to 250 °C. The heating/cooling rate was 10 °C/min, and the tests were carried out in a nitrogen atmosphere with a flow rate of 66 ml/min. The glass transition temperature (T_g), the cold crystallization temperature (T_{cc}) and enthalpy (ΔH_{cc}), and the melting temperature (T_m) and enthalpy (ΔH_m) were obtained from the second heating stage. Additionally, crystallinity (χ_c [%]) was calculated according to Equation (7):

$$\chi\,[\%] = \frac{|\Delta H_m| - |\Delta H_{cc}|}{|\Delta H_m^0| \cdot (1-w)} \cdot 100 \qquad (7)$$

where ΔH_m^0 is a theoretical value that represents the estimated melt enthalpy of a 100% crystalline PLA polymer, *i.e.* 93.7 J/g, where $1 - w$ is the PLA weight fraction.

2.3.5. Dynamical mechanical thermal characterization

Dynamical mechanical thermal analysis (DMTA) was carried out in a DMA1 dynamic analyzer from Mettler-Toledo (Schwerzenbach, Switzerland), working in single cantilever flexural conditions. Rectangular samples with dimensions 20×6×2.7 mm were subjected to a dynamic temperature sweep from –150 to 100 °C at a constant heating rate of 2 °C/min. The selected frequency was 1 Hz, and the amplitude of the cantilever flexural deformation was set to 10 µm.

2.3.6. Visual appearance characterization

The visual appearance of the PLA/TPF composites was assessed by colorimetric analysis using a colorimeter model KONICA CM-3600d Colorflex-DIFF2 from Hunter Associates Laboratory (Reston, Virginia, USA). Prior to measurements, the instrument was calibrated using a standard white tile and a light trap. CieLab color coordinates were measured and recorded. Measurements were taken in triplicate and averaged.

2.3.7. Water contact angle measurements

The distilled water contact angle in PLA/TPF composites was evaluated in order to assess their hydrophilicity. An Easy drop FM140 goniometer supplied by Krüss equipments (Hamburg, Germany) was used. Distilled water drops were deposited at random on the surface of impact test samples. At least 10 measurements were taken for each material.

2.3.8. Fourier transformed infrared spectroscopy (FTIR)

The chemical interactions present in the PLA/TPF composites were studied through the use of attenuated total reflection-Fourier transformed infrared spectroscopy (ATR-FTIR). Three spectra of each material were recorded by using a Bruker S.A Vector 22 (Madrid, Spain) coupled to a PIKE MIRacle™ single reflection diamond ATR accessory (Madison, Wisconsin, USA). 20 scans were taken and averaged for each measurement, between 4000 and 500 cm^{-1}, with a resolution of 2 cm^{-1}.

2.3.9. Biodegradability

The biodegradability of PLA/TPF composites was evaluated in compost soil conditions at a temperature of 58 °C and a relative humidity of 55% according to ISO 20200. 25×25×1 mm samples were placed in a textile mesh. Then they were buried in a solid synthetic wet soil prepared with 40 wt% sawdust, 30 wt% rabbit feed, 10 wt% corn starch, 10 wt% compost, 5 wt% sugar, 4 wt% of corn oil, and 1 wt% of urea. Samples were periodically extracted from the compost and cleaned with distilled water, then they were dried and weighted with an analytical balance model AG245 provided by Mettler-Toledo (Schwerzenbach, Switzerland) with an accuracy of 0.001 g. The percentage of weight loss was calculated using Equation (8):

$$\text{Weight loss} = \frac{w_0 - w_t}{w_0} \cdot 100\% \tag{8}$$

where w_0 is the initial dry weight of the sample and w_t is the weight of the sample after t burial time. All assays were carried out in triplicate to ensure more accuracy and reliability.

3. Results

3.1. Mechanical properties

Table 3 gathers the main mechanical parameters for PLA/TPF composites regarding the tensile test, the Shore D hardness test, and the Charpy impact test. As it can be seen, neat PLA shows an elastic modulus of 3761 MPa, a tensile strength of 56 MPa, and a very low elongation at break of 5.6%. These are typical values of a strong and brittle polymer. Very similar results were reported by Lascano *et al.* [27]. The incorporation of 10 wt% of TPF provokes a decrease in all tensile parameters, especially reducing the elongation at break of the composite(from 5.6 down to 3.3%). It is possible that TPF is provoking a stress concentration effect as a result of the formation of aggregates that act as stress concentrators [7]. Interestingly, the addition of TA into the PLA+10TPF composite drastically enhances its ductile properties, exhibiting an elongation at break of 194%, which is an impressive feat considering the extreme brittleness of the PLA+10TPF composite (3.3% elongation at break). On the other hand, a decrease in elastic modulus and tensile strength from 3420 and 37.4 down to 1804 and 11.1 MPa is observed. This proves the plasticizing effect that TA exerts over the composite, which is also a direct indicator of the good miscibility between PLA and TA, as predicted in the theoretical solubility parameter section. It is observed that when the proportion of TPF is increased, elongation at break is clearly decreased, so for the samples with 20 and 30 wt% of TPF, elongation at break is 156 and 104%, respectively. This is ascribed to the great number of lignocellulosic particles, which make the formation of stress concentrator aggregates more likely to happen [28]. Nevertheless, the reported values are still very impressive, considering the great amount of lignocellulosic filler contained in the PLA-based composites (30 wt%). In fact, tensile strength and the elastic modulus decrease with the increase in TPF, probably due to an excessive load of hard organic particles. This effect was also observed by Jorda-Reolid *et al.* [28] in biopolypropylene composites with 30 wt% of argan shell particles, who observed the formation of argan shell particles aggregate in the composites, which acted as stress concentrators. Finally, the plasticized PLA (PLA+20TA) shows the highest elongation at break registered within these composites (327.6%). This definitely proves the excellent plasticizing effect that TA provides to the PLA matrix, considering that PLA is extremely fragile (5.6% elongation at break), which increases the mobility of the polymer chains and makes them more flexible.

Regarding Shore D hardness, neat PLA shows a hardness of 79.8, which is very similar to the value reported by Lascano *et al.* [27]. The incorporation of TPF into the PLA matrix increases the hardness up to 82.0. This was expected, as TPF is a hard lignocellulosic filler, thus enhancing the hardness of the composite. Quiles-Carrillo *et al.* [29] also reported an increase in the Shore D hardness of PLA composites with orange peel flour. This increase in hardness is due to the intrinsic hardness of the filler, which is a lignocellulosic element with considerable crystallinity. The addition of the plasticizer to PLA and PLA/TPF composites clearly reduces their hardness,

Table 3. Summary of the mechanical parameters of the PLA/TPF composites regarding tensile test: tensile modulus (E), tensile strength (σ_{max}) and elongation at break (ε_b); Shore D hardness and impact strength.

Code	E [MPa]	σ_{max} [MPa]	ε_b [%]	Shore D hardness	Impact strength [kJ/m^2]
PLA	3761±787	56.0±1.9	5.6±0.5	79.8±3.3	1.8±0.2
PLA+10TPF	3420±470	37.4±3.6	3.3±0.5	82.0±1.4	1.8±0.5
PLA+10TPF+22.5TA	1804±328	11.1±1.5	194.4±12.0	71.6±3.8	3.1±0.3
PLA+20TPF+20TA	2159±251	8.4±1.6	156.6±13.6	74.6±2.3	4.3±0.9
PLA+30TPF+17.5TA	1976±375	6.8±0.5	104.0±17.7	70.8±1.3	4.2±1.1
PLA+20TA	1861±170	15.9±1.3	327.6±0.1	71.4±3.0	5.1±2.0

down to values in the range of 70–75, which is due to the plasticizing effect of TA and the enhancement of the mobility of PLA chains.

Finally, the impact strength results show that neat PLA presents an impact strength of 1.8 kJ/m^2, indicative of quite a fragile polymer. The addition of TPF to PLA does not vary this value, while the presence of the plasticizer in the polymer matrix clearly improves its absorption of impact energy up to values in the range of 3 to 5 kJ/m^2. Specifically, the sample with 20TA is the one that presents the highest impact strength (5.1 kJ/m^2). This is a direct consequence of the plasticizing effect, which improves the ductile properties of PLA.

3.2. Morphological properties

Figure 2 gathers the morphology of plasticized and unplasticized PLA/TPF cross-section samples by means of field emission scanning electron microscopy (FESEM) at a 500× magnification. Figure 2a shows the typical flat and uniform morphology of a resistant and brittle polymer such as PLA [30]. Figure 2b shows the addition of TPF into the PLA matrix, in which the presence of the lignocellulosic particles (black arrows) is clearly seen. The adhesion between the particles and the matrix seems to be good, as the gap between them is very narrow, thus indicating a certain affinity between both components. Nonetheless, as it was reported in the mechanical properties section, it seems that TPF particles have formed aggregates that act as stress concentrators, increasing the brittleness of PLA. On the other hand, as observed in Figures 2c–2e, the presence of the plasticizer in the matrix with TPF leads to a rougher surface with filament-like formations (indicative of a ductile fracture) (black circles) and even better interaction between TPF and PLA. This could be ascribed to a compatibilizing effect exerted by the plasticizer between TPF and PLA, as α-terpinyl acetate can act as a chemical bridge between lignocellulosic particles and the PLA matrix, considering that both plasticizer and PLA possess good miscibility, as studied in the theoretical solubility parameter section by means of the van Krevelen-Hoftyzer method. This improvement in adhesion is denoted by a very narrow and practically inexistent particle-matrix gap. Additionally, the increase in particle concentration from Figure 2c (10 wt%) to Figure 2e (30 wt%) is clearly observed, especially in the sample with 30 wt% TPF, where a higher number of particles is present in the matrix. Finally, Figure 2f shows the morphology of PLA/TA, where some filament-like structures can be observed. These structures are related to the ductile behavior observed in the mechanical characterization [31]. All in all, the results presented here match the mechanical properties exhibited in the previous section, concluding in a high ductility provided by the plasticizer and a higher strength provided by the TPF.

3.3. Thermal properties

Figure 3 shows all the DSC thermograms obtained for the PLA/TPF composites, while Table 4 gathers all the main thermal parameters extracted from those thermograms. The first thermal transition observed in the thermograms is the glass transition temperature (T_g). Neat PLA shows a typically high T_g value of 62.6 °C, which is indicative of a certain rigid material at room temperature [32]. The addition of TPF does not significantly vary the glass transition temperature of PLA. On the other hand, the addition of the plasticizer drastically decreases the T_g of the polymer matrix, especially the PLA+20TPF+20TA and PLA+20TA samples, which exhibit values of 44.0 and 41.6 °C, respectively. This is ascribed to the enhanced chain mobility that the plasticizer provides the PLA matrix, as T_g is a thermal parameter that depends on the mobility of the amorphous phase of the polymer [33]. Interestingly, the incorporation of TPF and TA led to the appearance of a cold crystallization peak in all the samples containing those components. This is ascribed to a heterogeneous nucleating effect, which provokes the appearance of several points from where crystallites start to grow [34]. The plasticized sample exhibits a considerable decrease in this peak; this fact is related to the enhanced mobility of PLA chains, which can arrange more easily (at a lower temperature). Regarding the melting point of the materials, neat PLA shows a melting temperature of 173.2 °C, which is a very typical value for this rigid polymer [35]. This value is slightly affected by the incorporation of the plasticizer, which reduces it down to 168, 171, and 169 °C for the PLA+20TPF+20TA, PLA+30TPF+17.5TA, and PLA+20TA samples, respectively. This effect is ascribed to an increase in the chain mobility of the polymer exerted by the plasticizer. Finally, the crystallinity of PLA was increased as a result of the addition of TPF and TA from a value of 5.2% for neat PLA up to 27.7 for the sample with 20 wt% TPF and

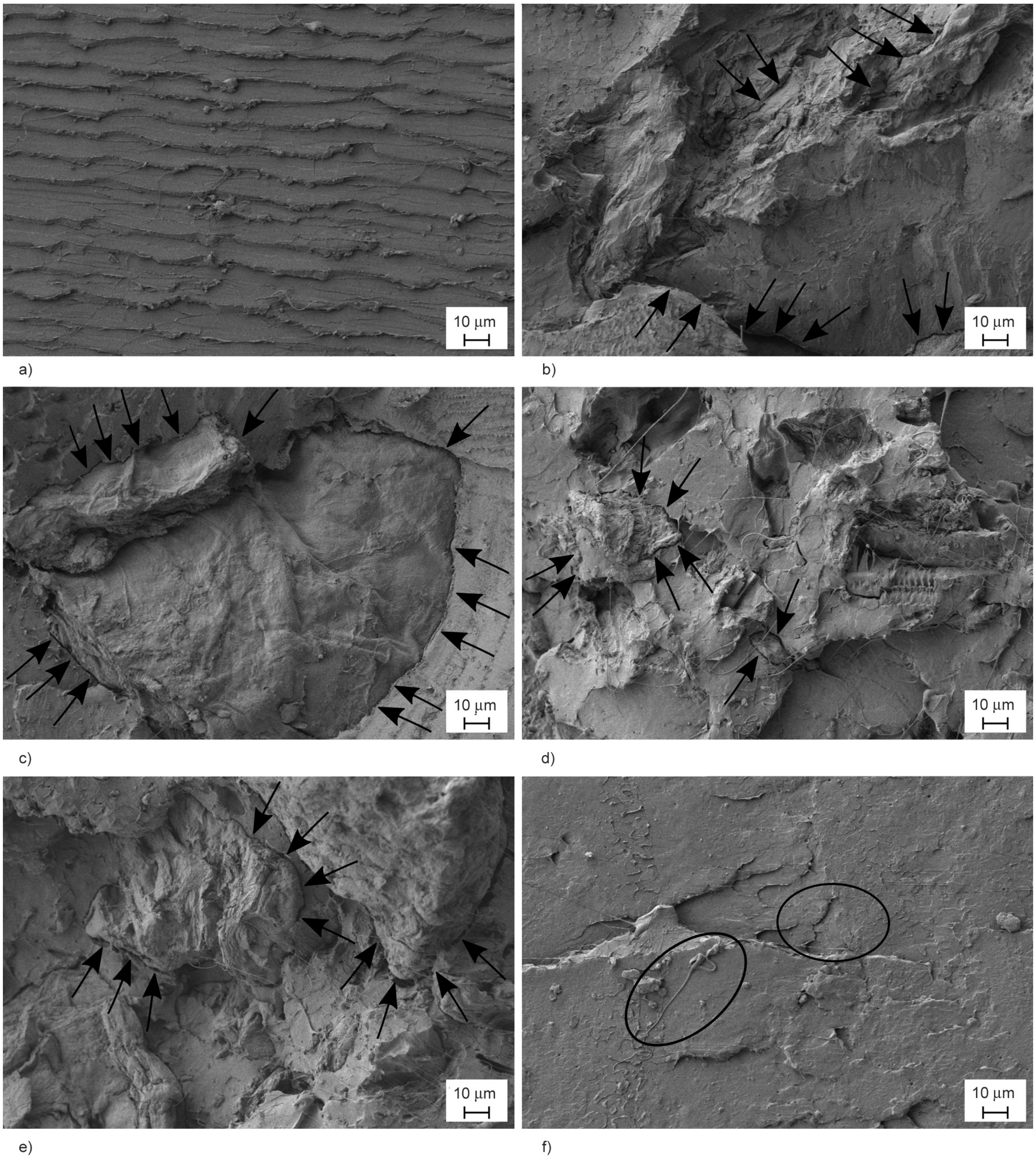

Figure 2. FESEM images at 500× magnification of the PLA/TPF composites: a) PLA; b) PLA+10TPF; c) PLA+10TPF+22.5TA; d) PLA+20TPF+20TA; e) PLA+30TPF+17.5TA and f) PLA+20TA.

20 phr TA, which can also be responsible for the observed mechanical performance. This effect is due to the aforementioned increase in chain mobility, which increases the crystallization rate of the amorphous phase of PLA, allowing it to crystallize at a lower cold crystallization temperature, as was observed in the PLA+20TPF+20TA and PLA+20TA samples. On the other hand, TPF also promotes the crystallization of PLA due to a heterogeneous nucleating effect. This effect promotes the distribution of TPF particles all along the polymer matrix, forming different points from which crystals start to grow [28]. The thermal degradation of the developed composites was studied by thermogravimetric analysis (TGA) and the first derivative of the thermograms (DTG). Figure 4 shows the TGA thermal degradation profiles and their first derivatives, while Table 5 gathers the main thermal parameters related to this analysis. First of all, the onset degradation temperature (the temperature at which 5% of the mass is lost)

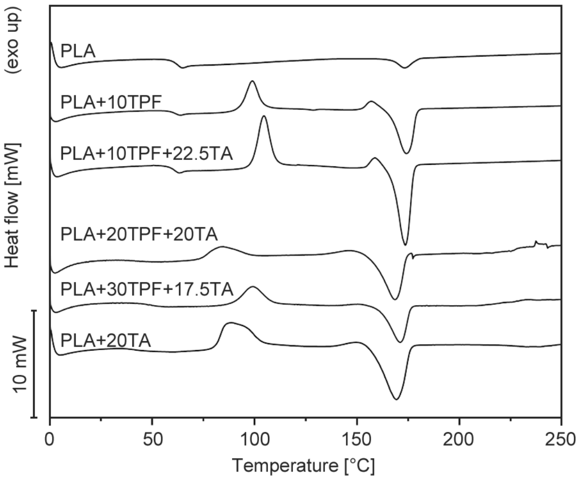

Figure 3. DSC thermograms of all the PLA/TPF samples.

of neat PLA stays at 305 °C, which is a very similar value that the one observed by Quiles-Carrillo *et al.* [7]. The addition of TPF clearly decreases this value down to 290 °C. This is ascribed to the relatively low thermal stability of the lignocellulosic filler, which, in turn, reduces the overall thermal stability of the composite. This fact occurs due to the thermal degradation of cellulose and lignin between 250 and 350 °C, as well as hemicellulose which degrades even at lower temperatures than cellulose [7]. With the introduction of the plasticizer into the polymer matrix, the thermal stability of the composites considerably decreases, showing values of the onset degradation temperature from 154 to 232 °C, far below the values reported for neat PLA and PLA/TPF. This phenomenon is clearly related to the volatility of the plasticizer (*i.e.*, α-terpinyl acetate is a typical component of some essential oils), which possesses a boiling point of approximately 220 °C. The volatility of the plasticizer is clearly detectable on the TGA thermograms, noted by a first mass loss step in the thermal degradation in all the plasticized composites, which occurs approximately at 220 °C, coinciding with the boiling point of the plasticizer. This decrease in thermal stability is also ascribed to enhanced chain mobility in PLA. A similar trend is observed for the maximum degradation peak temperature, although in this case, the decrease in thermal stability is not so acute, as the plasticizer has already been almost completely gone, reporting values in the range of 321–356 °C. In the case of residual weight, it is very close to zero in all

Table 4. Glass transition temperature (T_g), cold crystallization temperature (T_{cc}), cold crystallization enthalpy (ΔH_{cc}), melting temperature (T_m), melting enthalpy (ΔH_m), and degree of crystallinity (χ_c) of PLA/TPF plasticized and unplasticized composites obtained by differential scanning calorimetry (DSC).

Code	T_g [°C]	Tcc [°C]	ΔH_{cc} [J/g]	T_m [°C]	ΔH_m [J/g]	χ_c [%]
PLA	62.6±1.1	–	–	173.2±3.0	4.8±0.1	5.2±0.1
PLA+10TPF	61.6±0.9	99.1±2.0	27.1±0.5	173.9±2.2	50.2±0.6	27.6±0.3
PLA+10TPF+22.5TA	61.1±1.2	104.8±1.5	24.2±0.3	173.3±1.2	40.5±0.8	19.5±0.1
PLA+20TPF+20TA	44.0±0.8	83.7±1.3	10.7±1.0	168.3±1.0	31.3±0.6	27.7±0.2
PLA+30TPF+17.5TA	47.5±0.7	99.5±1.6	21.3±0.7	170.9±1.5	27.9±0.4	10.1±0.1
PLA+20TA	41.6±1.1	88.5±1.0	25.6±0.1	168.9±2.0	38.5±0.2	17.3±0.3

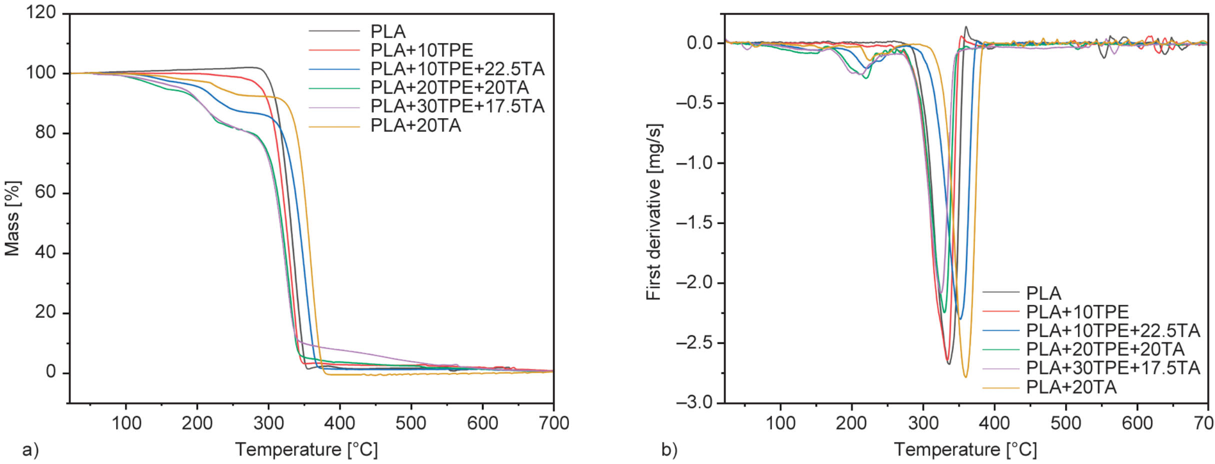

Figure 4. Thermogravimetric analysis (TGA) (a) and its first derivative of the plasticized and unplasticized PLA/TPF composites (b).

Table 5. Main thermal degradation parameters of PLA/TPF composites plasticized with TA in terms of the onset degradation temperature at a mass loss of 5 wt% ($T_{5\%}$), maximum degradation rate (peak) temperature (T_{deg}), and residual mass at 700 °C.

Code	$T_{5\%}$ [°C])	T_{deg} [°C]	Residual weight [%]
PLA	305.0±0.6	337.5±0.5	0.5±0.1
PLA+10TPF	290.0±0.4	332.0±0.3	0.9±0.1
PLA+10TPF+22.5TA	206.5±0.7	349.0±0.8	0.7±0.1
PLA+20TPF+20TA	154.0±0.6	330.5±1.2	0.5±0.1
PLA+30TPF+17.5TA	179.0±1.0	321.0±0.5	0.7±0.1
PLA+20TA	232.5±1.3	356.0±1.1	0.5±0.1

cases. This was expected as all the samples are organic and at 700 °C they are completely disintegrated.

3.4. Dynamic mechanical thermal properties

Figure 5a shows the storage modulus (E') variation of the different PLA-based composites with TPF, Figure 5b shows the dynamic damping factor (tan δ diagram of these composites, whereas Table 6 gathers the main thermomechanical parameters of the composites in which the glass transition temperature was calculated utilizing the tan δ criterion (peak maximum). The DMTA curve of PLA shows a glassy region comprised between –150 and 50 °C approximately. This region is characterized by a rigid behavior with a storage modulus of around 1500 MPa. Between 50–70 °C, a dramatic decrease (of at least two-three orders of magnitude) in the storage modulus can be seen, which is related to the glass transition region. Above 70 °C, the DMTA shows a rubbery plateau region characterized by a very low storage modulus. The glass transition temperature (T_g) can be assessed by several criteria, such as the onset of the storage modulus decrease, or what is more common, the peak maximum of the dynamic damping factor as seen in Figure 5b, resulting in a T_g for neat PLA of 63.9 °C. the addition of TPF lignocellulosic filler provides the expected behavior. In general, lignocellulosic fillers lead to more rigid polymers, which is reflected in DMTA by a shift of the characteristic DMTA curve of neat PLA to higher E' values, as observed in Figure 5a. As can be seen, the glass transition region is similar to that of neat PLA, but a slight decrease can be observed in the peak maximum of the dynamic damping factor (Figure 5b), with a T_g value of 60.4 °C. As the TPF increases, the corresponding DMTA curves are shifted to higher E' values, thus indicating more rigid materials are obtained (this is clearly observed at low temperatures, below –10 °C). Nevertheless, at room temperature, the plasticization effects are evident since the characteristic DMTA curves are shifted to lower E' values, thus indicating more flexible materials at room temperature. The combination of TPF with the terpene-based plasticizer leads to some synergistic effect since higher E' values are obtained, but a decrease in the T_g can be seen too with values comprised between 40–45 °C approximately.

PLA shows the lowest initial storage modulus, with a value of 1464 MPa at –100 °C. A very similar thermomechanical profile was observed by Lascano *et al.* [27]. The incorporation of TPF increases this value up to 1965 MPa, which coincides with what was observed in mechanical properties, as the hard lignocellulosic filler increases the rigidity of the

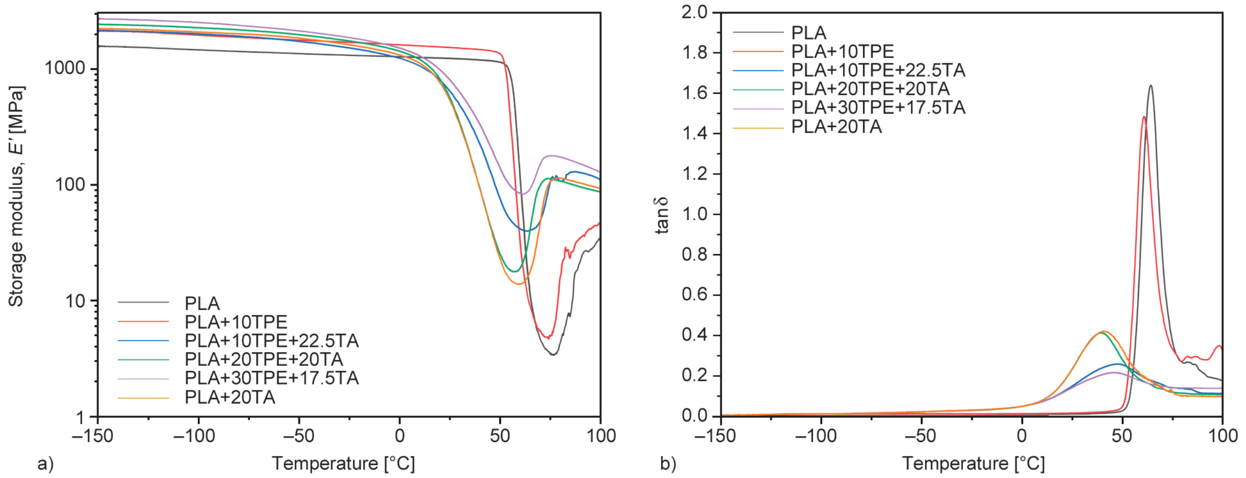

Figure 5. Thermomechanical diagrams of the plasticized and unplasticized PLA/TPF composites: a) storage modulus (E'); b) dynamic damping factor (tan δ).

Table 6. Dynamic-mechanical-thermal properties of PLA/TPF plasticized with α-terpinyl acetate (TA), at different temperatures.

Code	E' at –100 °C [MPa]	E' at 20 °C [MPa]	E' at 80 °C [MPa]	T_g [°C]
PLA	1464±45	1245±21	4±7	63.9±1.3
PLA+10TPF	1965±33	1551±27	16±9	60.4±2.2
PLA+10TPF+22.5TA	2013±28	798±25	108±5	46.2±2.1
PLA+20TPF+20TA	2280±32	811±30	108±7	39.9±1.7
PLA+30TPF+17.5TA	2534±40	982±27	174±8	46.5±1.5
PLA+20TA	2081±40	756±40	114±40	40.6±1.5

*The T_g has been measured using the tan δ peak maximum criterion.

polymer. Surprisingly, the addition of the plasticizer also increases the storage modulus in the temperature range between –150 and –10 °C, with values higher than 2000 MPa, probably due to some interaction between the plasticizer and the lignocellulosic filler below their characteristic T_g values. Nonetheless, as the temperature rises, the plasticized samples clearly decrease their storage modulus more rapidly as a result of the increased polymer chain mobility. Thus, it can be seen that at room temperature (20 °C approximately), the storage modulus of the plasticized samples is far lower than that of neat PLA and PLA/TPF (PLA presents a value of 1245 MPa, while the plasticized samples have values in the range 756–982 MPa). A sudden decrease in the storage modulus can be appreciated for all samples, which is indicative of their glass transition temperature, related to the mobility of the amorphous region of the polymer [36]. This thermal transition is more accurately observed in the tan δ plot, where it is indicated by a peak. As it was expected, the glass transition of neat PLA (peak maximum of the tan δ peak) and PLA/TPF occurs at higher temperatures than the plasticized samples. The glass transition of neat PLA is located at 63.9 °C, which is very close to the value reported in the DSC analysis. The glass transition of the unplasticized PLA/TPF composite is 60.4 °C. On the other hand, the plasticized samples exhibit values in the range of 40–46 °C; the samples with 20TA are the ones with the lowest T_g. This fact is ascribed to the enhanced mobility of the amorphous region of the polymer as a result of the presence of α-terpinyl acetate molecules, which diminish the activation energy barrier for segmental relaxations of the surrounding polymer molecules to occur [37]. These results perfectly match the findings reported in DSC, where the effect of the plasticizer was reflected in the glass transition values. It is also worth noting the cold crystallization process, which can be observed by DMTA by an increase in the storage modulus at temperatures above 60–70 °C, as seen in Figure 5a. Neat PLA does not show this process, which is consistent with the previous DSC results on thermal properties. On the other hand, both the TPF and the terpene-based plasticizer promote cold crystallization since TPF has a nuclear effect, and the plasticizer increases the chain mobility, both phenomena having a positive effect on increasing crystallinity, which confirms the previously reported results by DSC.

3.5. Visual aspect and color properties

Color and luminance are essential parameters when it comes to wood plastic composites, as these parameters determine the visual appearance of the composites and the degree of similarity with several kinds of wood. Figure 6 shows the visual aspect of all the developed composites, while Table 7 gathers the main color parameters regarding the CieLab color space. As can be inferred from the appearance of the samples, both the samples of neat PLA and PLA with the plasticizer show clear colors, being the plasticized PLA composite more opaque than neat PLA. This is also seen in luminance values, where these two samples present higher values of luminance than the samples with TPF, going from values of approximately 45 down to values of 22–25, respectively. This is because luminance stands for white (higher values) and black (lower values). As expected, TPF samples possess darker brownish colors that resemble that of certain woods, which gives them great application as plastic materials that can substitute wood-based materials [3].

Regarding color coordinates a^* (green for negative values and red for positive values) and b^* (blue for negative values and yellow for positive values), the samples that have TPF in their composition present higher positive a^* values than neat PLA and plasticized PLA. This is ascribed to a characteristic brown

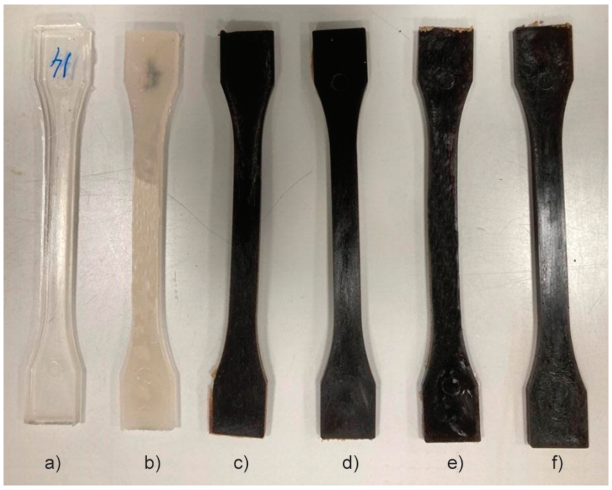

Figure 6. Visual appeal of the samples: a) PLA; b) PLA+20TA; c) PLA+10TPF d) PLA+10TPF+22.5TA; e) PLA+20TPF+20TA and f) PLA+30TPF+17.5TA.

Table 7. Luminance and color coordinates (L^*, a^*, b^*) of the PLA/TPF composites plasticized with α-terpinyl acetate.

Code	L^*	a^*	b^*
PLA	46.16±0.87	0.08±0.04	0.72±0.15
PLA+10TPF	25.05±0.21	1.55±0.12	1.78±0.05
PLA+10TPF+22.5TA	22.25±0.19	0.74±0.35	1.72±0.18
PLA+20TPF+20TA	23.57±0.24	1.14±0.14	1.13±0.10
PLA+30TPF+17.5TA	23.61±0.13	1.15±0.14	1.29±0.37
PLA+20TA	44.22±0.01	–0.41±0.06	1.59±0.07

color that approaches the red color, which is located in the positive region of a^*. On the other hand, with regard to b^* color coordinate, all samples except for neat PLA possess positive values superior to 1. This is related to an approach of the samples to the yellow color, located on the positive side of the chromatic space. These values can be verified by Figure 6, where the plasticized sample presents a more yellow-like color than neat PLA; while the TPF samples present dark brown colors, which are closer to yellow than the color of neat PLA.

3.6. Wettability

Wood plastic composites present a great trend to absorb water due to the presence of highly hydrophilic components in their composition (*i.e.*, cellulose, hemicellulose, pectin, and lignin) [38]. This is considered one of the main drawbacks of this kind of material. Figure 7 gathers the contact angle measurements carried out in each one of the samples, with the objective of studying the wettability of the developed composites. Neat PLA presents a contact angle of 87.3° [39], which is a typical value for this polymer, and it is indicative of a hydrophobic behavior, considering the hydrophilic threshold of Vogler located at 65° [40]. The addition of 10 wt% TPF decreased the water contact angle of PLA down to 83°. This is ascribed to the presence of the aforementioned lignocellulosic components, which are highly polar molecules and possess a great concentration of hydroxyl groups (–OH). These functionalities give TPF a great affinity for water, as they make it possible to create hydrogen bonds. The addition of α-terpinyl acetate slightly decreases the contact angle in relation to the PLA/10TPF sample as a result of the free volume it provides to PLA. As expected, the contact angle decreases as the proportion of TPF is superior. This is corroborated by a contact angle of 63.4° for the sample with 30 wt% of TPF, which makes more –OH functionalities to be readily available to interact with water. Finally, the sample of PLA/TA also demonstrates the increased free volume provided by the plasticizer, as the contact angle decreases from 87 down to 81.4° in relation to neat PLA.

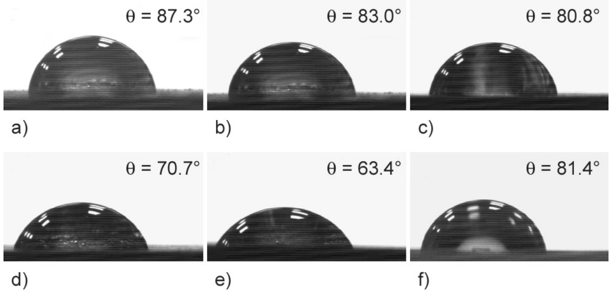

Figure 7. Contact angle measurements of the PLA/TPF composites: a) PLA; b) PLA+10TPF; c) PLA+10TPF+22.5TA; d) PLA+20TPF+20TA; e) PLA+30TPF+17.5TA and f) PLA+20TA.

3.7. Chemical characterization

Figure 8 shows the FTIR spectra of neat PLA, PLA with TPF, and the plasticized and unplasticized PLA/TPF composites. First of all, neat PLA presents a common spectrum for this polymer. One of the main representative bands is located at 1751 cm^{-1} and it is ascribed to the C=O stretching. The bands between 1250 and 1000 cm^{-1} are also significant and are related to the ester C–O and C–O–C stretching vibrations. The bands in the range 1500–1300 cm^{-1} are indicative of symmetric and antisymmetric deformational vibrations of the C–H bond in methyl groups [29]. The incorporation of TPF into the polymer matrix did not significantly change the spectra of PLA. On the other hand, the incorporation of

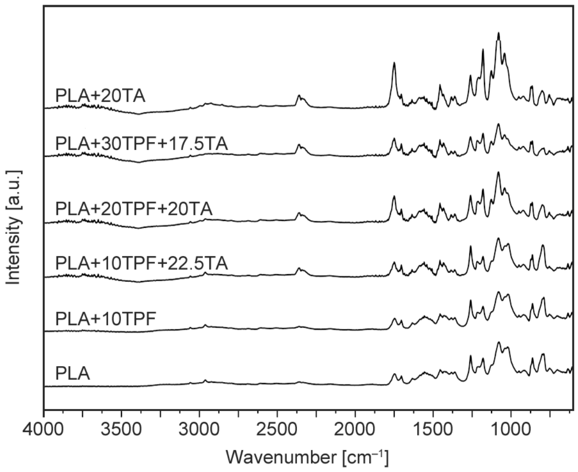

Figure 8. FTIR diagrams of neat PLA and the plasticized and unplasticized PLA/TPF composites.

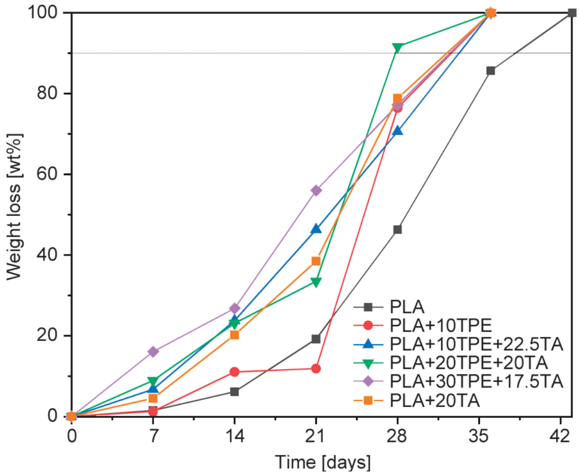

Figure 9. Disintegration profile of the plasticized and unplasticized PLA/TPF composites over time.

α-terpinyl acetate induced some interesting changes in the spectra. In the region of 3400 cm^{-1} a small band can be observed for all the plasticized samples, which could be related to the presence of hydrogen bonding between TA and PLA or TA with lignocellulosic compounds in TPF [41]. Then, another peak appears at approximately 1450 cm^{-1}, which is ascribed to C=O stretching in the ester group present in TA; this peak becomes more intense in the PLA/TA sample as the concentration of plasticizer is higher in this composite. Finally, a small peak at around 1200 cm^{-1} appears due to the rocking vibration of the C–H bond.

3.8. Disintegration test

The biodegradability of the samples was assessed through the disintegration test in controlled compost soil. Figure 9 shows the disintegration evolution (mass loss) all over 6 weeks in which the samples were buried in controlled compost soil (the black line at 90% is indicative of the disintegration goal). On the other hand, Figure 10 illustrates the visual appearance of the samples throughout the disintegration process. It can be seen that after an incubation time of 5 weeks, all samples except for neat PLA have achieved complete disintegration, while PLA completely disintegrates after 6 weeks. This fact demonstrates the biodegradability of all the herein-presented composites. The disintegration profile of neat PLA is very similar to the one observed by Quiles-Carrillo *et al.* [29], who also observed the complete disintegration of neat PLA and PLA/orange peel flour samples. This suggests that both the lignocellulosic filler (TPF) and the plasticizer enhance the biodegradability of PLA. Interestingly, in spite of the fact that all samples except PLA fully disintegrate in 5 weeks, the plasticized samples present a higher disintegration rate in the first weeks. This is probably ascribed to the low thermal stability of the α-terpinyl acetate, which provokes a higher weight loss rate [42]. Moreover, the plasticizer seems to catalyze the hydrolysis of PLA, making it easier for bacteria to decompose the polymer. The visual appearance of the samples supports these results, where it can be seen how in the second week all materials have undergone severe weight loss. A color change in neat PLA and PLA+20TA can be observed from a white clear color to a darker tonality as a result of the disintegration process. Therefore, it can be concluded that all samples are effectively biodegradable and that TPF and the plasticizer contribute to reducing the amount of time necessary to achieve 100% disintegration. Probably due to the hydrophilic behavior of both components, as demonstrated in the contact angle analysis.

4. Conclusions

In this work, environmentally friendly and fully biodegradable composites have been obtained by combining a PLA polymer matrix, tangerine peel flour (TPF) as a reinforcing filler, and α-terpinyl acetate as a natural origin plasticizer to improve toughness. The materials herein presented have proved to possess excellent mechanical performance in terms of ductility. Especially thanks to the plasticizing effect of α-terpinyl acetate, which allowed to achieve elongations at break superior to 300% in the case of the PLA+20TA sample, and elongations at break close

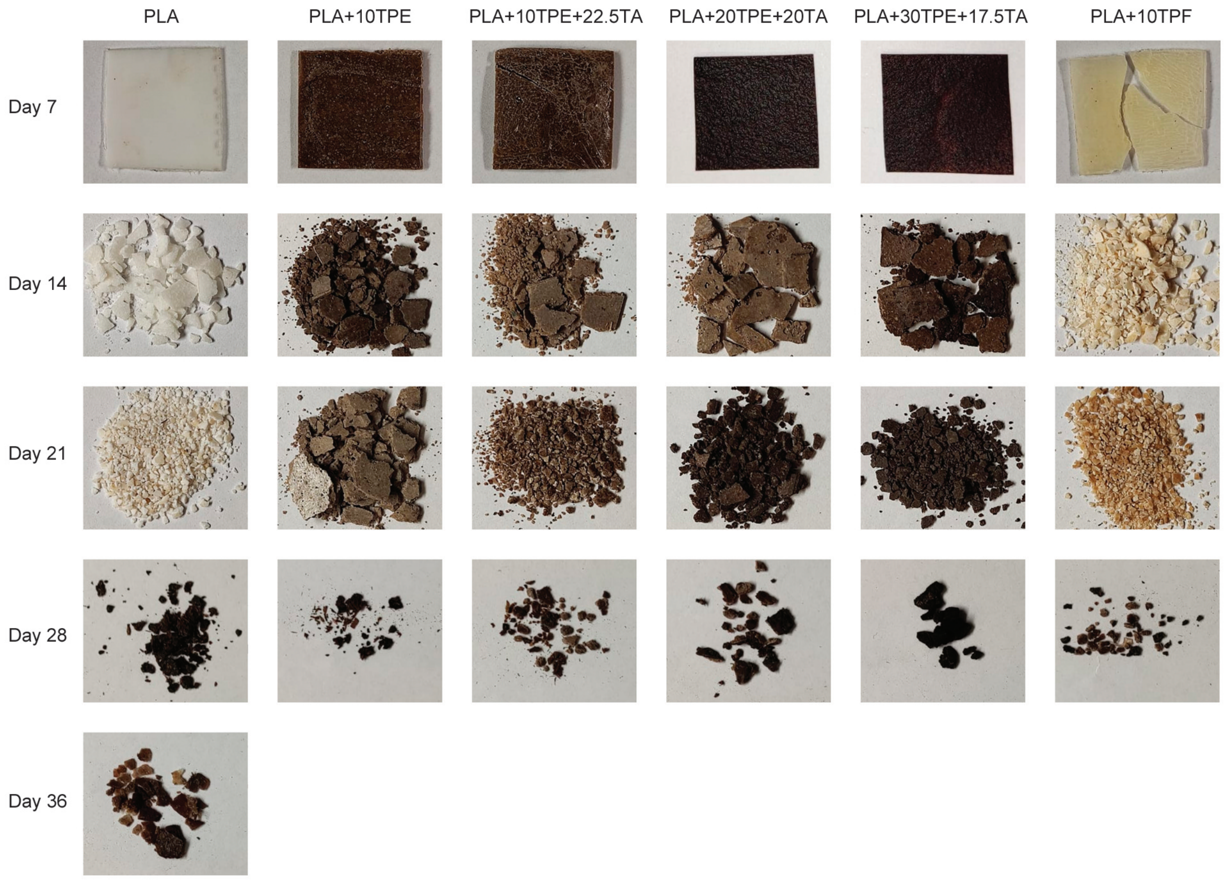

Figure 10. Visual appearance of the disintegration process of PLA/TPF composites (25×25×1 mm samples) over time.

to 200% in the case of PLA+10TPF+22.5TA. The performance of PLA+10TPF+22.5TA is quite an interesting result considering that TPF is a hard and rigid filler that would normally increase the brittleness of PLA. This good interaction between PLA and the plasticizer was confirmed by theoretical solubility parameter determination, which concluded that, indeed both elements were highly compatible. The mechanical characterization was verified by FESEM, where filament-like structures were observed, which were indicative of effective plasticization. In terms of thermal characterization, α-terpinyl acetate drastically reduced the glass transition temperature of PLA, which gave the composites greater ductility and better processability, reaching glass transition temperatures around 40 °C, which is a noticeable reduction considering that neat PLA presents a glass transition temperature of 63 °C. Additionally, it was observed how the plasticizer increased the thermal disintegration rate of the composites due to its volatility, decreasing the thermal stability of the materials in the temperature range of 200–300 °C. The composites presented characteristic dark brown colors, similar to that of wood, making them perfect for substituting wood-based products. Moreover, the presence of TPF and the acetate increased the affinity of PLA for water, according to contact angle measurements, reaching contact angle values of 60°. Finally, the disintegration test proved that all the developed samples were completely biodegradable after 5 weeks under controlled compost soil conditions, surpassing the biodegradability of neat PLA (100% disintegration after 6 weeks), which greatly enhances the environmentally friendly nature of these materials, altogether with the natural origin of all of their components. All in all, this work opens up a new research line centered on the use of tangerine wastes as lignocellulosic fillers for polymers. The great effectiveness of TA as a plasticizer has also been demonstrated, which could be tried in other brittle polymers, such as poly(3-hydroxybutyrate-co-3-hydroxyhexanoate) (PHBH) in order to evaluate if it is capable of increasing its ductility.

Acknowledgements

This research is a part of the grant PID2020-116496RB-C22 funded by MCIN/AEI/10.13039/501100011033. Authors also thank Generalitat Valenciana-GVA, grant number AICO/2021/025, and CIGE/2021/094 for supporting this work. J. Gomez-Caturla wants to thank Generalitat Valenciana-GVA, for his FPI grant (ACIF/2021/185) and grant FPU20/01732 funded by MCIN/AEI/10.13039/ 501100011033 and by ESF Investing in your future. J. Ivorra-Martinez wants to thank FPU19/01759 grant funded by MCIN/AEI/10.13039/501100011033 and by ESF Investing in your future. Microscopy Services at UPV are also acknowledged for their help in collecting and analyzing images.

References

[1] Khan M. Z. R., Srivastava S. K., Gupta M. K.: A state-of-the-art review on particulate wood polymer composites: Processing, properties and applications. Polymer Testing, **89**, 106721 (2020).
https://doi.org/10.1016/j.polymertesting.2020.106721

[2] Petchwattana N., Naknaen P., Narupai B.: A circular economy use of waste wood sawdust for wood plastic composite production: Effect of bio-plasticiser on the toughness. International Journal of Sustainable Engineering, **13**, 398–410 (2020).
https://doi.org/10.1080/19397038.2019.1688422

[3] Gomez-Caturla J., Balart R., Ivorra-Martinez J., Garcia-Garcia D., Dominici F., Puglia D., Torre L.: Biopolypropylene-based wood plastic composites reinforced with mango peel flour and compatibilized with an environmentally friendly copolymer from itaconic acid. ACS Applied Polymer Materials, **1**, 4398–4410 (2022).
https://doi.org/10.1021/acsapm.2c00373

[4] Botta L., Titone V., Mistretta M. C., la Mantia F. P., Modica A., Bruno M., Sottile F., Lopresti F.: PBAT based composites reinforced with microcrystalline cellulose obtained from softwood almond shells. Polymers, **13**, 2643 (2021).
https://doi.org/10.3390/polym13162643

[5] Bashar D., Yaro A. S., Yawas D. S., Aku S. Y.: Long term thermo-mechanical prediction of banana stem particulate reinforced PVC composite as piping material. Pakistan Journal of Engineering and Applied Sciences, **23**, 8–16 (2018).

[6] Banerjee J., Singh R., Vijayaraghavan R., MacFarlane D., Patti A. F., Arora A.: Bioactives from fruit processing wastes: Green approaches to valuable chemicals. Food Chemistry, **225**, 10–22 (2017).
https://doi.org/10.1016/j.foodchem.2016.12.093

[7] Quiles-Carrillo L., Montanes N., Sammon C., Balart R., Torres-Giner S.: Compatibilization of highly sustainable polylactide/almond shell flour composites by reactive extrusion with maleinized linseed oil. Industrial Crops and Products, **111**, 878–888 (2018).
https://doi.org/10.1016/j.indcrop.2017.10.062

[8] Nampoothiri K. M., Nair N. R., John R. P.: An overview of the recent developments in polylactide (PLA) research. Bioresource Technology, **101**, 8493–8501 (2010).
https://doi.org/10.1016/j.biortech.2010.05.092

[9] Luna C. B., Siqueira D. D., Araújo E. M., Wellen R. M.: Annealing efficacy on PLA. Insights on mechanical, thermomechanical and crystallinity characters. Momento, **62**, 1–17 (2021).
https://doi.org/10.15446/mo.n62.89099

[10] Villadiego K. M., Tapia M. J. A., Useche J., Macías D. E.: Thermoplastic starch (TPS)/polylactic acid (PLA) blending methodologies: A review. Journal of Polymers and the Environment, **30**, 75–91 (2022).
https://doi.org/10.1007/s10924-021-02207-1

[11] Patil S. S., Jena H. M.: Performance assessment of polyvinyl chloride films plasticized with citrullus lanatus seed oil based novel plasticizer. Polymer Testing, **101**, 107271 (2021).
https://doi.org/10.1016/j.polymertesting.2021.107271

[12] Martin O., Avérous L.: Poly(lactic acid): Plasticization and properties of biodegradable multiphase systems. Polymer, **42**, 6209–6219 (2001).
https://doi.org/10.1016/S0032-3861(01)00086-6

[13] da Silva J. M. F., Soares B. G.: Epoxidized cardanol-based prepolymer as promising biobased compatibilizing agent for PLA/PBAT blends. Polymer Testing, **93**, 106889 (2021).
https://doi.org/10.1016/j.polymertesting.2020.106889

[14] Yu R-L., Zhang L-S., Feng Y-H., Zhang R-Y., Zhu J.: Improvement in toughness of polylactide by melt blending with bio-based poly(ester)urethane. Chinese Journal of Polymer Science, **32**, 1099–1110 (2014).
https://doi.org/10.1007/s10118-014-1487-9

[15] Wypych G.: Handbook of plasticizers. ChemTec Publishing, Toronto (2004).

[16] Ojha P., Thapa S.: Quality evaluation of biscuit incorporated with mandarin peel powder. Scientific Study & Research. Chemistry & Chemical Engineering, Biotechnology, Food Industry, **18**, 19–30 (2017).

[17] Ordóñez-Santos L. E., Esparza-Estrada J., Vanegas-Mahecha P.: Ultrasound-assisted extraction of total carotenoids from mandarin epicarp and application as natural colorant in bakery products. Lwt, **139**, 110598 (2021).
https://doi.org/10.1016/j.lwt.2020.110598

[18] Mackenzie L. S., Tyrrell H., Thomas R., Matharu A. S., Clark J. H., Hurst G. A.: Valorization of waste orange peel to produce shear-thinning gels. Journal of Chemical Education, **96**, 3025–3029 (2019).
https://doi.org/10.1021/acs.jchemed.8b01009

[19] Farahmandfar R., Tirgarian B., Dehghan B., Nemati A.: Comparison of different drying methods on bitter orange (*Citrus aurantium* L.) peel waste: Changes in physical (density and color) and essential oil (yield, composition, antioxidant and antibacterial) properties of powders. Journal of Food Measurement and Characterization, **14**, 862–875 (2020).
https://doi.org/10.1007/s11694-019-00334-x

[20] Hejna A., Barczewski M., Kosmela P., Aniśko J., Mysiukiewicz O., Marć M.: Mandarin peel as an auspicious functional filler for polymer composites. Macedonian Journal of Chemistry and Chemical Engineering, **1**, 89–106 (2021).
https://doi.org/10.20450/mjcce.2021.2236

[21] Rathinavel S., Saravanakumar S. S.: Development and analysis of polyvinyl alcohol/orange peel powder biocomposite films. Journal of Natural Fibers, **18**, 2045–2054 (2021).
https://doi.org/10.1080/15440478.2019.1711285

[22] Fehlberg J., Lee C-L., Matuana L. M., Almenar E.: Orange peel waste from juicing as raw material for plastic composites intended for use in food packaging. Journal of Applied Polymer Science, **137**, 48841 (2020).
https://doi.org/10.1002/app.48841

[23] Chowdhury S., Kumar S.: Alpha-terpinyl acetate: A natural monoterpenoid from *Elettaria cardamomum* as multi-target directed ligand in Alzheimer's disease. Journal of Functional Foods, **68**, 103892 (2020).
https://doi.org/10.1016/j.jff.2020.103892

[24] van Krevelen D. W., te Nijenhuis K.: Properties of polymers: Their correlation with chemical structure; Their numerical estimation and prediction from additive group contributions. Elsevier, Amsterdam (2009).

[25] Auras R. A., Lim L-T., Selke S. E., Tsuji H.: Poly(lactic acid): Synthesis, structures, properties, processing, and applications. Wiley, New York (2011).
https://doi.org/10.1002/9780470649848

[26] Brüster B., Adjoua Y-O., Dieden R., Grysan P., Federico C. E., Berthé V., Addiego F.: Plasticization of polylactide with myrcene and limonene as bio-based plasticizers: Conventional vs. reactive extrusion. Polymers, **11**, 1363 (2019).
https://doi.org/10.3390/polym11081363

[27] Lascano D., Moraga G., Ivorra-Martinez J., Rojas-Lema S., Torres-Giner S., Balart R., Boronat T., Quiles-Carrillo L.: Development of injection-molded polylactide pieces with high toughness by the addition of lactic acid oligomer and characterization of their shape memory behavior. Polymers, **11**, 2099 (2019).
https://doi.org/10.3390/polym11122099

[28] Jorda-Reolid M., Gomez-Caturla J., Ivorra-Martinez J., Stefani P. M., Rojas-Lema S., Quiles-Carrillo L.: Upgrading argan shell wastes in wood plastic composites with biobased polyethylene matrix and different compatibilizers. Polymers, **13**, 922 (2021).
https://doi.org/10.3390/polym13060922

[29] Quiles-Carrillo L., Montanes N., Lagaron J. M., Balart R., Torres-Giner S.: On the use of acrylated epoxidized soybean oil as a reactive compatibilizer in injection-molded compostable pieces consisting of polylactide filled with orange peel flour. Polymer International, **67**, 1341–1351 (2018).
https://doi.org/10.1002/pi.5588

[30] Barczewski M., Mysiukiewicz O., Matykiewicz D., Kloziński A., Andrzejewski J., Piasecki A.: Synergistic effect of different basalt fillers and annealing on the structure and properties of polylactide composites. Polymer Testing, **89**, 106628 (2020).
https://doi.org/10.1016/j.polymertesting.2020.106628

[31] Ivorra-Martinez J., Peydro M., Gomez-Caturla J., Boronat T., Balart R.: The potential of an itaconic acid diester as environmentally friendly plasticizer for injection-molded polylactide parts. Macromolecular Materials and Engineering, **307**, 2200360 (2022).
https://doi.org/10.1002/mame.202200360

[32] Zhorina L. A., Iordanskii A. L., Rogovina S. Z., Grachev A. V., Yakhina A. R., Prut E. V., Berlin A. A.: Thermal characterization and sorption of Fe^{III} ion by ternary polylactide–poly-3-hydroxybutyrate–chitosan compositions. Mendeleev Communications, **31**, 104–106 (2021).
https://doi.org/10.1016/j.mencom.2021.01.032

[33] Xuan W., Odelius K., Hakkarainen M.: Tunable polylactide plasticizer design: Rigid stereoisomers. European Polymer Journal, **157**, 110649 (2021).
https://doi.org/10.1016/j.eurpolymj.2021.110649

[34] Gao X., Qi S., Yang B., Su Y., Li J., Wang D.: Synergistic effect of plasticizer and nucleating agent on crystallization behavior of polylactide during fused filament fabrication. Polymer, **215**, 123426 (2021).
https://doi.org/10.1016/j.polymer.2021.123426

[35] Demchenko V., Kobylinskyi S., Iurzhenko M., Riabov S., Vashchuk A., Rybalchenko N., Zahorodnia S., Naumenko K., Demchenko O., Adamus G., Kowalczuk M.: Nanocomposites based on polylactide and silver nanoparticles and their antimicrobial and antiviral applications. Reactive and Functional Polymers, **170**, 105096 (2022).
https://doi.org/10.1016/j.reactfunctpolym.2021.105096

[36] Mathew A. P., Oksman K., Sain M.: Mechanical properties of biodegradable composites from poly lactic acid (PLA) and microcrystalline cellulose (MCC). Journal of Applied Polymer Science, **97**, 2014–2025 (2005).
https://doi.org/10.1002/app.21779

[37] DeFelice J., Lipson J. E.: The influence of additives on polymer matrix mobility and the glass transition. Soft Matter, **17**, 376–387 (2021).
https://doi.org/10.1039/D0SM01634A

[38] Hiasa S., Iwamoto S., Endo T., Edashige Y.: Isolation of cellulose nanofibrils from mandarin (*Citrus unshiu*) peel waste. Industrial Crops and Products, **62**, 280–285 (2014).
https://doi.org/10.1016/j.indcrop.2014.08.007

[39] Prus-Walendziak W., Kozlowska J.: Design of sodium alginate/gelatin-based emulsion film fused with polylactide microparticles charged with plant extract. Materials, **14**, 745 (2021).
https://doi.org/10.3390/ma14040745

[40] Vogler E. A.: Water and the acute biological response to surfaces. Journal of Biomaterials Science, Polymer Edition, **10**, 1015–1045 (1999). https://doi.org/10.1163/156856299X00667

[41] Debabhuti N., Neogi S., Mukherjee S., Dhar A., Sharma P., Vekariya R. L., Sarkar M. P., Tudu B., Bhattacharyya N., Bandyopadhyay R.: Development of QCM sensor to detect α-terpinyl acetate in cardamom. Sensors and Actuators A: Physical, **319**, 112521 (2021). https://doi.org/10.1016/j.sna.2020.112521

[42] Arrieta M. P., López J., Rayón E., Jiménez A.: Disintegrability under composting conditions of plasticized PLA–PHB blends. Polymer Degradation and Stability, **108**, 307–318 (2014). https://doi.org/10.1016/j.polymdegradstab.2014.01.034